ELSEVIER

Palaeogeography, Palaeoclimatology, Palaeoecology 198 (2003) 39–52

PALAEO

www.elsevier.com/locate/palaeo

A coupled climate–ice sheet modeling approach to the Early Cenozoic history of the Antarctic ice sheet

Robert M. DeConto [a,*], David Pollard [b]

[a] Department of Geosciences, University of Massachusetts, Amherst, MA 01003, USA
[b] EMS Environment Institute, Pennsylvania State University, University Park, PA 16802, USA

Received 2 October 2002; accepted 3 March 2003

Abstract

The sudden, widespread glaciation of Antarctica and the associated shift toward colder temperatures near the Eocene–Oligocene boundary (~34 Ma) represents one of the most fundamental reorganizations of the global climate system recognized in the geologic record. This glacial inception and the subsequent evolution of the early East Antarctic Ice Sheet (EAIS) are simulated using a new, coupled global climate–dynamical ice sheet model accounting for the paleogeography, greenhouse gas concentrations, changing orbital parameters, and varying ocean heat transport. Suites of long (10^5 yr) climate–ice sheet simulations are used to investigate the effects of declining atmospheric CO_2, compared to those of the tectonic opening of Southern Ocean gateways and the timing of mountain uplift in the Antarctic interior. In contrast to the established paradigm for the glaciation of Antarctica, which centers on the opening of the Southern Ocean gateways and the 'thermal isolation' of the continent, our results show that declining Cenozoic pCO_2 may have played the dominant role. First, small isolated ice caps formed on the highest Antarctic plateaus. Then, as a CO_2 threshold between ~3× and 2× pre-industrial level (PAL) was crossed, height–mass balance feedbacks were initiated during orbital periods with cold austral summers, triggering much larger, highly dynamic terrestrial ice sheets. As CO_2 continued to decline, these isolated ice caps eventually merged into a permanent continental-scale EAIS. In our model, neither the opening of the Southern Ocean gateways nor mountain uplift significantly affected the timing of the major ice sheet transition, given a scenario of gradually declining CO_2 from 4× to 2× PAL over 10 million years around the Eocene–Oligocene boundary.

Keywords: Antarctica; Ice sheets; Oligocene; Paleoclimate; Drake Passage

1. Introduction

Antarctica has been located over southern polar latitudes since the Early Cretaceous (Lawver et al., 1992), yet is thought to have remained mostly ice-free, vegetated, and with mean annual temperatures above freezing until the initial, sudden growth of the East Antarctic Ice Sheet (EAIS) near the Eocene–Oligocene boundary (Barrett, 1996; Flower, 1999). The evidence for rapid cooling and East Antarctic glaciation comes mainly from the marine $\delta^{18}O$ record, in which the gradual cooling from the presumably ice-free warmth

* Corresponding author. Tel.: +1-413-545-3426; Fax: +1-413-545-1200.
E-mail addresses: deconto@geo.umass.edu (R.M. DeConto), pollard@essc.psu.edu (D. Pollard).

0031-0182/03/$ – see front matter © 2003 Elsevier B.V. All rights reserved.
doi:10.1016/S0031-0182(03)00393-6

of the Early Tertiary to the cold 'icehouse' of the Late Cenozoic is punctuated by a sudden ~1.5‰ rise in benthic $\delta^{18}O$ values at ~34 Ma (Zachos et al., 2001; Zachos et al., 1996). Comparison of high-resolution foraminiferal stable isotope and Mg/Ca from Late Eocene and earliest Oligocene deep-sea sediment have shown that approximately half of the Eocene–Oligocene $\delta^{18}O$ shift occurred within a brief ~50-ky period (Lear et al., 2000; Zachos et al., 2001), representing the sudden growth of a continental-scale EAIS. More direct evidence of cooling and sudden glaciation, provided by offshore and terrestrial geologic studies, include the record of circum-Antarctic ice rafted debris (IRD) (Zachos et al., 1992), a shift in the clay composition of circum-Antarctic sediments from smectite to chlorite and illite (Ehrmann and Mackensen, 1992) and the paleobotanical record of Antarctic vegetation, indicating the loss of warm-temperate vegetation and the increased dominance of other types more typical of high latitude environments (Askin, 1997; Birkenmajer and Zastawniak, 1989; Francis, 1999). Glaciation is believed to have begun in the East Antarctic continental interior, discharging mainly via the Lambert Graben to Prydz Bay, with the Transantarctic Mountains restricting ice flow toward the Ross Sea until the ice sheets became larger in the Middle Oligocene (Barrett, 1996). Paleogene Antarctic ice sheets are likely to have been temperate, highly dynamic (Barrett et al., 1987; Denton et al., 1991; Hambrey et al., 1991; Zachos et al., 1992) and paced by Milankovitch orbital parameters (Naish et al., 2001; Zachos et al., 1996) in much the same way as the Late Cenozoic ice sheets of the Northern Hemisphere.

The glaciation of East Antarctica is often attributed to the tectonic opening of the ocean gateways between Antarctica and Australia (Tasmanian Passage), and Antarctica and South America (Drake Passage), leading to the organization of the Antarctic Circumpolar Current (ACC) and the 'thermal isolation' of Antarctica (Exon et al., 2001; Kennett, 1977). However, direct linkages between the formation of an ACC and the sudden growth of East Antarctic ice near the Eocene–Oligocene boundary remain ambiguous. Ocean General Circulation Model (OGCM) simulations testing the effect of an open vs. closed Drake Passage support a linkage between Southern Ocean tectonics and Antarctic glaciation, by showing that the formation of an ACC reduces southward oceanic heat convergence by as much as 20% and cools high latitude sea surface temperatures (SSTs) by several degrees, (or less) in the zonal mean (Mikolajewicz et al., 1993; Nong et al., 2000; Toggweiler and Bjornsson, 2000; Toggweiler and Samuels, 1995). However, these ocean model studies lacked realistic atmospheric components, so the effects on Antarctic climate (and ice growth) are unknown. Bice et al. (2000) found somewhat larger changes in an OGCM driven by uncoupled Atmospheric General Circulation Model (AGCM) climates, with southern ocean heat transport decreasing by ~50% from 40 to 33 Ma. Again, the effect on atmospheric climate is unknown, but their larger oceanic response suggests that details in basin geometry may be important. Global Climate Model (GCM) studies using prescribed SSTs to represent open vs. closed Drake Passage conditions show a modest role for changes in ocean heat transport in the formation of an Antarctic ice sheet (Oglesby, 1989), and suggest the possibility that warmer SSTs are more favorable for ice sheet growth, by increasing snowfall in the continental interior (Oglesby, 1989; Prentice and Mathews, 1991). Furthermore, while most tectonic reconstructions place the opening of the Tasmanian Passage close to the Eocene–Oligocene boundary, Drake Passage did not open until several million years later (Lawver and Gahagan, 1998), and may not have provided a significant deep water passage until the Miocene (Barker and Burrell, 1977).

Antarctic elevation is another potentially important factor in ice sheet initiation (Huybrechts, 1993; Oglesby, 1989), via its effect on snow accumulation area, and the influence of mountains and outlet troughs on ice drainage. Dynamical 3-D ice sheet models have been used to test the sensitivity of EAIS dynamics to lowered continental topography (Huybrechts, 1993) and changes in the elevation of individual Transantarctic Mountain blocks (Kerr and Huybrechts, 1999). While Huybrechts (1993) showed a large sensitivity to an

imposed climate change on a uniformly flattened continent (due to enhanced sensitivity to snow line fluctuations), Kerr and Huybrechts (1999) found only a local response to the uplift individual mountain blocks, but concluded that interior ice thickness and surface gradients were sensitive to the development of wide and deep outlet troughs and changing drainage patterns.

Alternatively, the Cenozoic decline of atmospheric CO_2 may have played an important role in Paleogene cooling and Antarctic glaciation. Most estimates of Early Cenozoic CO_2 mixing ratios are between 2 and 5 times modern values, falling through the Cenozoic until reaching near-modern values sometime in the Neogene (Berner and Kothavala, 2001; Pearson and Palmer, 2000; Retallack, 2002). The cooling caused by declining pCO_2 would have gradually lowered annual snowline elevations until they intersected extensive regions of high Antarctic topography. Once some threshold was reached, feedbacks related to snow/ice–albedo and ice sheet height–mass balance (Abe-Ouchi and Blatter, 1993; Birchfield et al., 1982; Crowley et al., 1994; Maqueda et al., 1998) could have initiated rapid ice sheet growth during orbital periods favorable for the accumulation of glacial ice (i.e. those producing cool austral summers).

To test the relative importance of changing atmospheric CO_2, orbital parameters, ocean heat transport, and mountain uplift in the nucleation, development and fluctuations of the early EAIS, we have developed a new, coupled GCM–dynamical ice sheet model, specifically designed for ice sheet initiation experiments over long (orbital) time scales. Most prior ice sheet modeling studies of ancient Antarctic ice sheets have used empirical parameterizations based on modern climatologies for their surface mass balance forcing (Huybrechts, 1993; Kerr and Huybrechts, 1999). While these models are well suited for testing the response of ice sheets to changes in bedrock topography and different temperature and precipitation scenarios, they do not explicitly test the sensitivity of the coupled climate–cryosphere system to climatic forcing factors, such as changing greenhouse gas concentration, orbital periods, or ocean circulation. An alternative approach, and the one adopted here, uses a GCM, responding to evolving Paleogene boundary conditions and climatic forcing in three dimensions, to provide the meteorological input for our dynamical ice sheet model experiments. In our model scheme, coupling between the climate and ice sheet model components attempts to capture important climate–ice sheet feedbacks, while maintaining the computational efficiency required to run simulations long enough to be relevant on geological timescales. Results of some longer integrations (10 Ma) than shown here are described in DeConto and Pollard (2003). A model of deforming sediment under the ice can be added to the ice sheet model and used to predict coastal sediment discharge fluxes, as described in Pollard and DeConto (2003).

2. Models

The GCM component of our model is GENESIS (version 2.1) (Pollard and Thompson, 1997; Thompson and Pollard, 1997), with specific modifications to provide realistic surface mass-balance forcing for a 3-D, dynamical ice sheet model. The atmospheric component of GENESIS has 18 vertical layers and a spectral resolution of T31 ($\sim 3.75° \times 3.75°$), coupled to $2° \times 2°$ surface models including a non-dynamical 50-m slab ocean model with dynamical sea ice, and multi-layer models of soil, snow and vegetation. The slab ocean model captures the seasonal thermal capacity of the ocean's mixed layer, transporting heat as a linear diffusion down the local ocean temperature gradient as a function of latitude (based on modern estimates of ocean heat transport) and the zonal fraction of land vs. sea. This GCM produces realistic snowfall, melt and mass balances over the present-day Greenland and Antarctic ice sheets (Thompson and Pollard, 1997) and reasonable values for the Last Glacial Maximum (Pollard, 2000; Pollard and Thompson, 1997).

A 3-D ice sheet model of ice dynamics and local bedrock response is asynchronously coupled to the GCM, allowing feedbacks between the ice sheet and atmospheric model components. Rele-

vant monthly mean meteorologic fields used in the calculation of net annual surface ice mass balance (surface air temperature and precipitation) are horizontally interpolated and lapse-rate adjusted from the GCM to the much finer (40×40 km) ice sheet model grid. A computationally economical positive degree-day parameterization is used to calculate ablation potential from the monthly mean climatology provided by the GCM (Ritz et al., 1997), with allowances for diurnal cycles and the refreezing of meltwater (using early springtime melt to saturate the winter snowpack before it becomes mobile).

We use a standard 3-D dynamic ice sheet model, following the established lineage of Huybrechts (1993; 1990), Ritz et al. (1997), and others. The ice sheet evolves under the influence of ice flow, surface mass balance, and basal melting. Ice sheet flow is mainly by shear under its own weight, following the shallow ice approximation. The ice sheet grid is polar stereographic, with a 40×40 km grid size. There are ten unequally spaced vertical levels in the ice. An alternating direction implicit scheme is used for ice advection, with time-implicit, tri-diagonal Newton–Raphson contributions from all terms, allowing a basic timestep of 10 years. Ice temperatures are predicted mainly for their effect on ice rheology and basal conditions, and are influenced by ice advection, vertical diffusion, surface temperatures, and shear frictional heating. Vertical diffusive temperature profiles are also predicted through the upper ~2 km of bedrock, using 6 unequal levels, and a uniform geothermal heat flux of 0.9 microcalories/cm^2/s. There are no ice shelves; all ice is removed (calves) seaward of the continental shorelines. Thus, the glacial initiation of West Antarctica, which requires ice shelves joining West Antarctic islands (Fig. 1a) to the East Antarctic mainland, is not simulated here, but is postponed to future work. The asthenospheric response to ice load is a simple, local relaxation towards isostacy with a time scale of 5000 years. Lithospheric response is modeled by linear elastic deformation (Brotchie and Sylvester, 1969).

Boundary conditions for our Eocene–Oligocene climate–ice sheet simulations are based on a 34-Ma paleogeography, including reconstructions of shorelines, topography and vegetation superposed on a global tectonic model (Hay et al., 1999) and rotated to their 34-Ma positions. Ice-free Antarctic topography is reconstructed from a 5-km digital database of ice surface and bedrock topography (Bamber and Bindschadler, 1997), isostatically relaxed to ice-free equilibrium and interpolated to the ice sheet model grid (Fig. 1a). While the use of modern, isostatically equilibrated bedrock topography is not ideal for Eocene–Oligocene ice sheet simulations, the detailed paleotopography of Antarctica is not well known. Here, we assume that most of the broad-scale topographic features, such as the Transantarctic Mountains, were in place by the Paleogene (Fitzgerald, 1992). As described below, we test the sensitivity of ice sheet initiation to the uplift of the Gamburtsev Mountains; an area of high relief in the continental with a poorly constrained geologic/uplift history.

3. Results

3.1. CO_2 sensitivity

Our first set of experiments was designed to find the highest threshold value of atmospheric CO_2 that would allow the growth of an EAIS (Fig. 1). Assuming summer temperature (ablation) is the most important limitation to ice sheet initiation, an initial orbital configuration producing the coldest possible Antarctic summers (low obliquity, high eccentricity, and aphelion corresponding to austral summer) was applied to our GCM–ice sheet model (see Fig. 3a). Five experiments were performed, using the 34-Ma boundary conditions described above, with values of atmospheric CO_2 set at 8× pre-industrial (2240 ppm), 4×CO_2 (1120 ppm), 3×CO_2 (840 ppm), 2×CO_2 (560 ppm), and 1×CO_2 (280 ppm). First, the GCM is run to seasonal equilibrium for 25 years, with 34-Ma boundary conditions, a coldest austral summer orbit (Fig. 3a), and no initial ice. The saved meteorological fields, averaged over the last 10 years of the simulation are then used to integrate the ice sheet model for 10 000 years, updating the surface mass balance calculations every

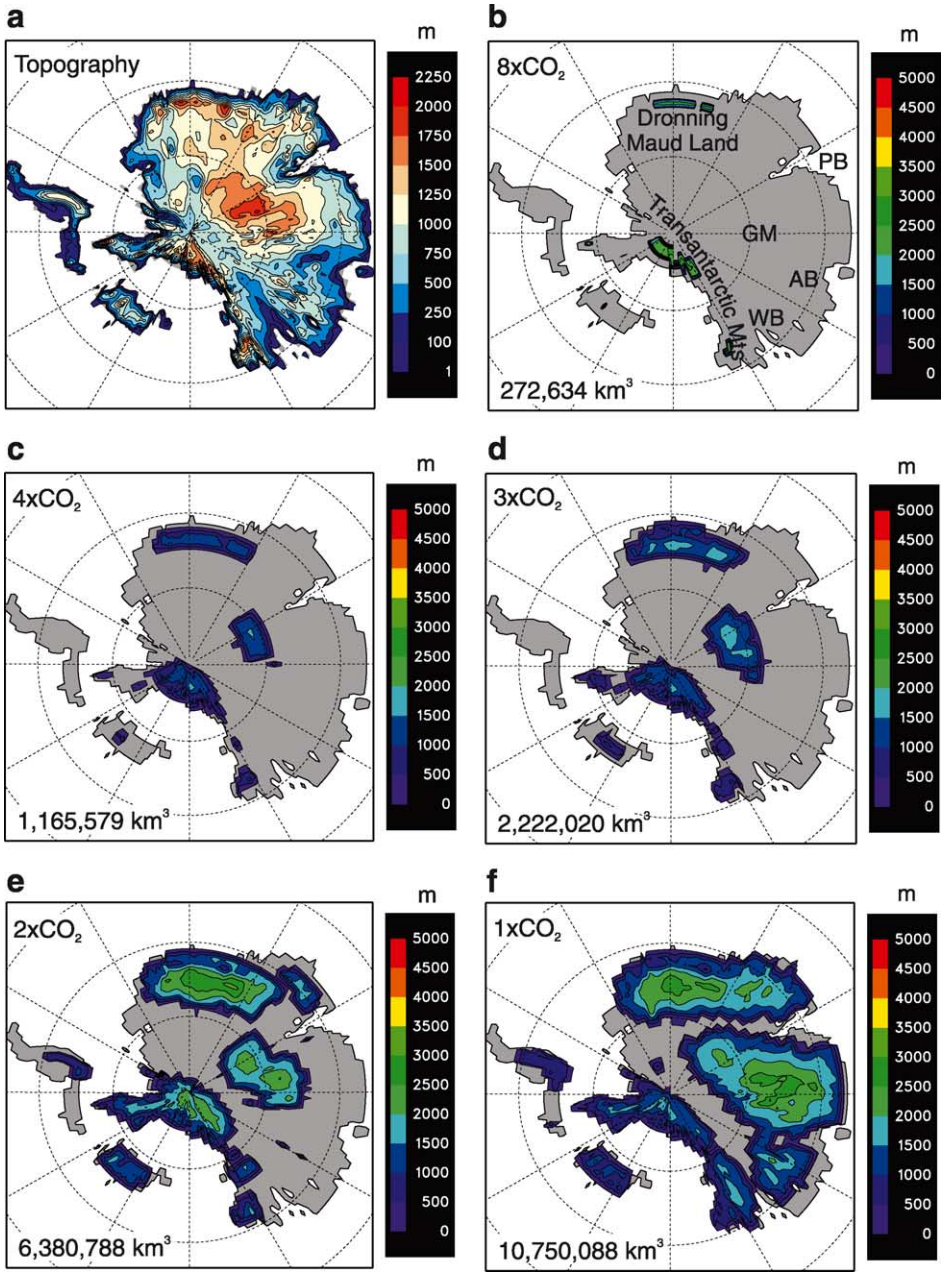

Fig. 1. (a) Early Cenozoic ice-free Antarctic topography (m above sea level) in our 34-Ma reconstruction (see text). (b) Abbreviated place names mentioned in the text: AB, Aurora Basin; DML, Dronning Maud Land; GM, Gamburtsev Mountains; LG, Lambert Graben; PB, Prydz Bay; TAM, Transantarctic Mountains; WB, Wilkes Basin; WL, Wilkes Land. (b)–(f) Ice sheet thickness (m) after 10 000 years of integration of the ice sheet model starting with no ice, driven by invariant GCM climates with different CO_2 levels. Each GCM solution used the same set of orbital parameters yielding coldest possible austral summers (see Fig. 3a). (b) $8\times CO_2$, 2240 ppmv. (c) $4\times CO_2$, 1120 ppmv. (d) $3\times CO_2$, 840 ppmv. (e) $2\times CO_2$, 560 ppmv. (f) $1\times CO_2$, 280 ppmv.

200 years to account for changing ice elevations. Because these experiments examine only the initial ice sheet growth, only one coupling step is taken. At $8\times CO_2$, small glaciers form in the Transantarctic Mountains and on the highest elevations of Dronning Maud Land. At $4\times$ and $3\times CO_2$, significant, yet isolated ice caps form in both Dronning Maud Land and in the Gamburtsev Mountain region. Rapid ice growth in the $2\times CO_2$ simulation (Fig. 1e) is attributed to the initiation of a height–mass balance feedback (Abe-Ouchi and Blatter, 1993; Birchfield et al., 1982; Crowley et al., 1994; Maqueda et al., 1998), suggesting a CO_2-ice sheet initiation threshold has been crossed. In the $1\times CO_2$ experiment (Fig. 1f), rapid glaciation produces three large ice caps, nearly coalescing into a continental ice sheet within a brief 10-ky period.

Some of the AGCM climates driving the ice sheet changes are illustrated in Fig. 2. The upper panels show modern Antarctica from the model's control simulation, in good agreement with observations (Thompson and Pollard, 1997). The middle panels shows the combined effects of removing the modern ice (warming, wetting) and an extreme cold austral summer orbit (summer cooling). With this orbit, there are quite extensive high-elevation areas that remain below freezing in summer, allowing large ice sheets to nucleate and expand as in Fig. 1f. The lower panels show the same no-ice Cenozoic climate but with $3\times CO_2$. Now the subfreezing areas in summer are much smaller, limited to the very highest plateaus, and elsewhere summer melt limits ice growth to the small isolated caps shown in Fig. 1d. Precipitation also changes (Fig. 2, right panels), but the effect on ice budgets is small compared to melt due to summer temperature changes (left panels), as is usual for ice sheets with inland ablation zones like the Quaternary Laurentide and Eurasian.

3.2. 40-ky runs ($3\times$ and $2\times CO_2$)

While the 10-ky CO_2 sensitivity experiments are useful for examining the potential for ice sheet initiation under ideal and fixed orbital parameters, longer simulations are required to determine the potential for the ice sheets to survive periods of increased ablation potential as orbital cycles progress (Fig. 3). To do this, long-term orbital experiments were performed using an iterative, asynchronous GCM-ice sheet coupling scheme, and a synthetic orbital cycle described below. The coupling procedure is as follows: (1) the GCM is run to seasonal equilibrium as above, with 34-Ma boundary conditions, no ice, and a cold austral summer orbit (Fig. 3a); (2) the ice sheet model is run for 10 000 years using saved meteorological fields averaged over the last 10 years of the previous GCM run; and (3) the GCM is rerun with updated orbital parameters and ice sheet geometry. This iteration is repeated five times, representing one idealized (40-ky) obliquity cycle and one half of an idealized (80-ky) eccentricity cycle (Fig. 3b). While the coupling between the ice sheet model and GCM is temporally coarse, it provides the required efficiency for completing long, coupled GCM-ice sheet integrations.

The 40-ky orbital cycle and its climatological effects are described in Fig. 3. The orbital sequence is synthetic, allowing it to be smoothly linked for longer runs (see below). While the periodicities are idealized, ranges of eccentricity and obliquity are within the range of those calculated over the last 5 my (Berger and Loutre, 1991). As shown in Fig. 3d, the orbital configuration at time-step 1 (red curve) maintains warmest monthly mean temperatures near 0°C, whereas the orbital configuration at the next asynchronous time-step 10 ky later (blue curve) places Antarctica into a strongly negative snow mass balance, illustrating increased sensitivity to Milankovitch orbital variations during geologic periods with higher than present atmospheric CO_2 and small Antarctic ice sheets. Precession, usually considered an important low-latitude forcing mechanism during the last 50 ky, when eccentricities have been relatively low, has a large high latitude effect on Antarctic snow budgets during periods of high eccentricity.

Asynchronous coupled 40-ka integrations were run for two atmospheric CO_2 levels of $3\times$ and $2\times$ PAL (Fig. 4). At $3\times CO_2$, small, isolated ice caps form over coastal mountains in Dronning Maud Land, in response to orographically lifted

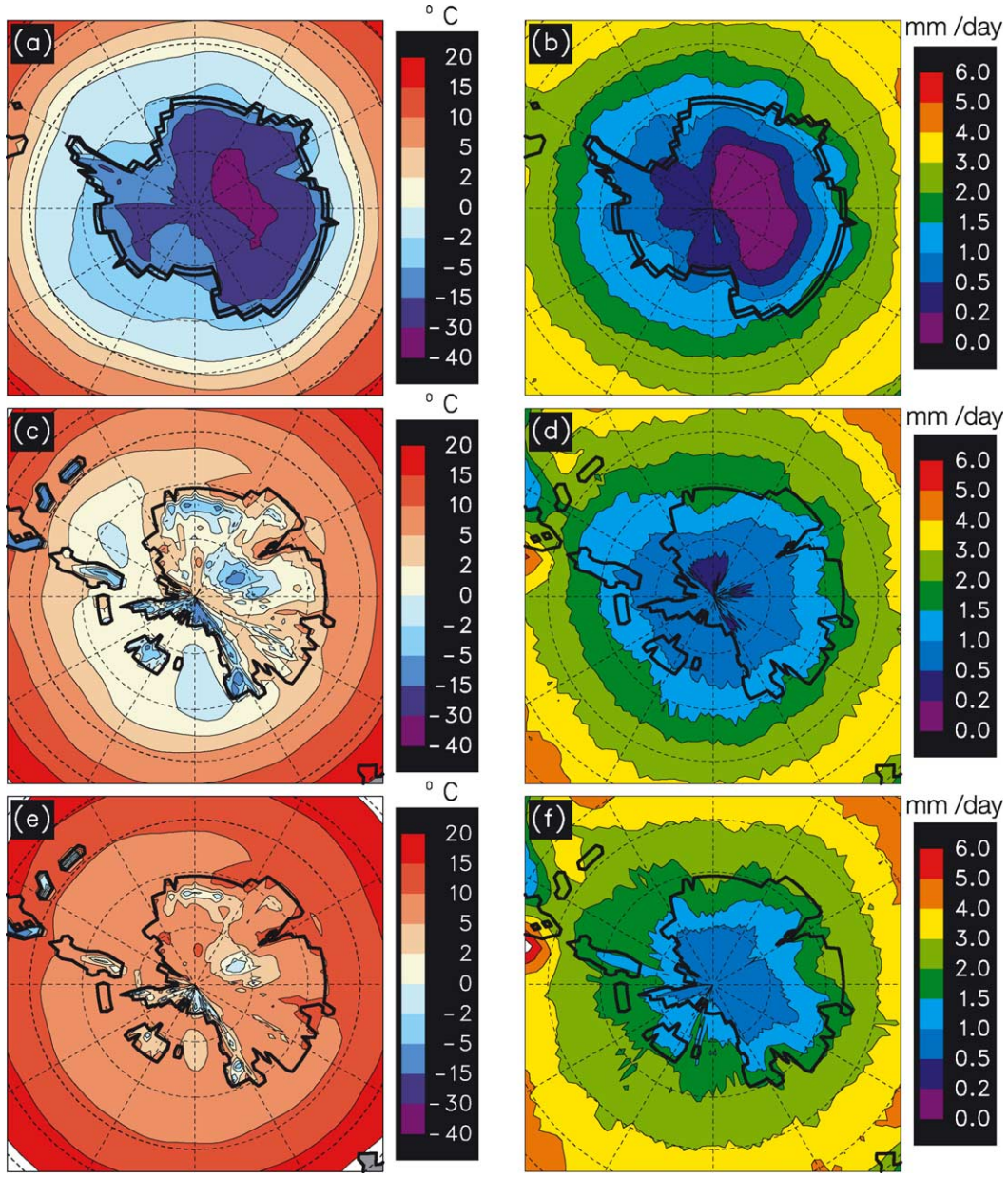

Fig. 2. GCM January surface-air temperature in °C (left panels), and annual precipitation in mm/day (right panels), over the Antarctic region for for three different climates: (a,b) present day with modern Antarctic ice sheet; (c,d) ~34 Ma, with no ice, $1\times CO_2$, and coldest austral summer orbit; (e,f) as (c,d) except with $3\times CO_2$.

maritime moisture from extra-tropical cyclones and associated fronts producing high winter snowfall, over the polar plateau/Gamburtsev Mountain region in the continental interior, and along the Transantarctic Mountains. While winter snowfall is generally higher in the $3\times CO_2$ simulation, it is outpaced by summer ablation in most of the continental interior, especially during periods of high obliquity and precession placing perihelion during austral summer. Thus, the rapid

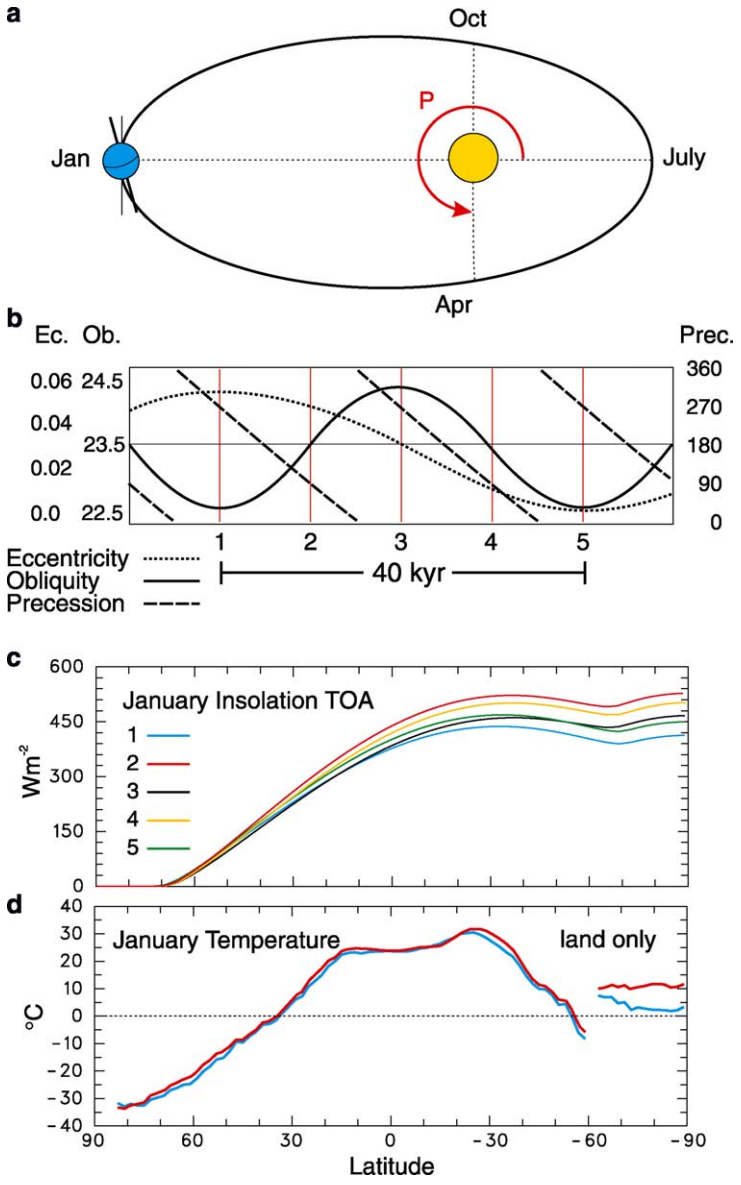

Fig. 3. Synthetic orbital variations used in our GCM-ice sheet integrations and their potential effect on snow accumulation on an initially ice-free Antarctica at $2\times CO_2$. (a) Schematic representation of the orbital configuration used in the CO_2 sensitivity tests (Fig. 1) and at the beginning of each 40-ky sequence, yielding coldest possible austral summers (orbit 1 in the next panel). *P*, the prograde angle between perihelion and the Northern Hemispheric vernal equinox, is related to the precession cycle and determines the month when the Earth is at aphelion. (b) The 40-ka synthetic orbital sequence used in our long GCM-ice sheet simulations. Numbers 1–5 correspond to the orbital time-steps used in the coupled GCM–ice sheet integrations. Orbit 1 corresponds to the diagram in (a), with maximum eccentricity (0.05), minimum obliquity (22.5°), and $P = 270°$. Precession, obliquity and eccentricity have sinusoidal periodicities of 20, 40 and 80 ka, respectively, so that eccentricity completes a half cycle during the run. (c) Austral summer (January) insolation at the top of the model atmosphere, shown at each orbital time-step (1–5). (d) The effect of orbital parameters at time-step 1 (blue) and 2 (red) on the warmest month (January) zonal mean temperatures at $2\times CO_2$ with an ice-free Antarctica.

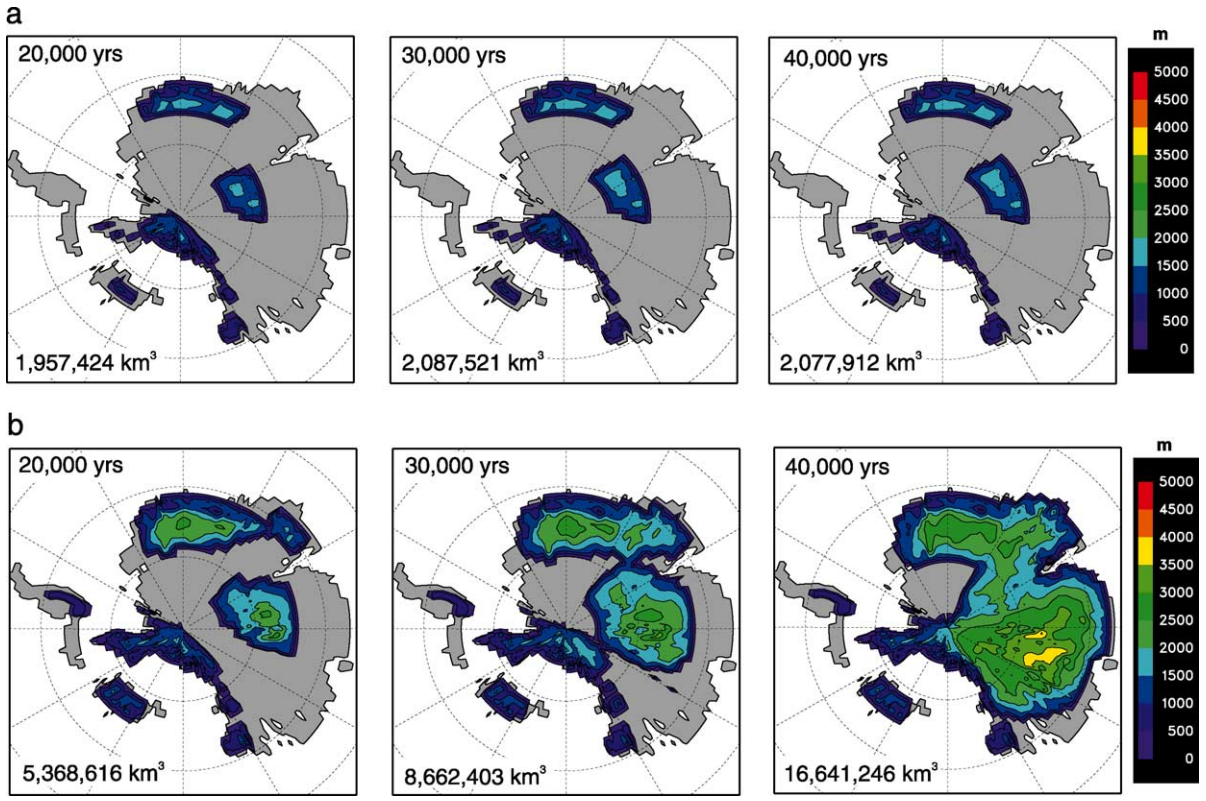

Fig. 4. Ice sheet thicknesses (m) at 10-ky intervals, from asynchronous GCM-ice sheet integrations with different atmospheric CO_2 values, over one synthetic 40-ky obliquity cycle starting with no ice. Total ice volumes are indicated at the bottom left of each panel. Three 10-ky time-steps are shown for each run, illustrating the evolution of ice sheet geometry: (a) with $3\times CO_2$; (b) with $2\times CO_2$. The sequence shown in (a) and (b) are extensions of the simulations shown in Fig. 1d,e, respectively. Note the reduction in ice volume from 10 to 20 ky, due to the effect of precession and increased obliquity in the second orbital time-step (Fig. 3b,c).

growth of a continental-scale ice sheet is prevented until CO_2 drops below $3\times CO_2$.

For $2\times CO_2$, Fig. 4b shows that during an orbital period producing minimal summer insolation, net snow accumulation remains positive while snow/ice albedo and height mass–balance feedbacks are initiated, allowing a continental-scale EAIS to form within a single 40-ky obliquity cycle. In this scenario, the ice sheet is initiated in two main areas centered over the higher elevations of Dronning Maud Land and the Gamburtsez Mountain region, eventually coalescing near the Lambert Graben and flowing down the local bedrock gradient toward Prydz Bay and the Wilkes and Aurora Basins. Within 40-ky, the ice sheet reaches sea level around most of the continental margin, with the potential for producing IRD like that recognized in the earliest Oligocene marine record (Zachos et al., 1992).

3.3. 400-ka runs (Drake Passage)

The simulations described above show that the threshold CO_2 value for height–mass balance feedbacks to trigger large ice sheet growth in the nominal model lies between $2\times$ and $3\times$ PAL. In this section, the robustness of this result is tested in the light of other possible, long-term climate/ice sheet forcings, namely the opening of oceanic gateways such as the Drake Passage, and the uplift of the Gamburtsev Mountains, a broad mountain range in the continental interior (see Fig. 1a)

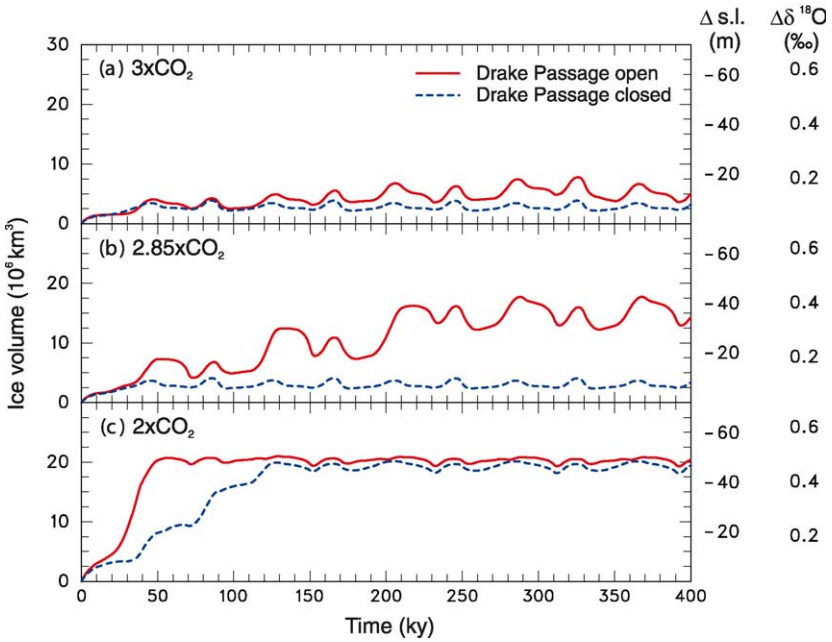

Fig. 5. Total Antarctic ice volumes over the 400-ky integrations of the ice sheet model, forced with weighted combinations of the stored GCM climates from shorter 40-ky cycles; red curves show ice volumes using the nominal GCM representing an open Drake Passage and blue curves use GCM solutions with increased Southern Hemispheric ocean heat transport representing closed Drake Passage (see text): (a) with $3\times CO_2$; (b) with '$2.85\times CO_2$', using appropriate weights of the GCM solutions for the other two CO_2 values; (c) with $2\times CO_2$. Equivalent changes in sea-level (Δs.l.) and the mean isotopic composition of the ocean ($\Delta\delta_w$) are also shown, with Δs.l. calculated according to the global land area fraction in our 34-Ma paleogeography (0.731) and $\Delta\delta_w$ calculated assuming 0.0091 per 1 m change of sea level.

with a poorly known geologic history. For these simulations, somewhat longer runs are needed to allow the ice sheets to approach equilibrium over many orbital cycles. We extend the length of the ice sheet model simulations to 400 000 years, by repeatedly using the stored sets of 5 GCM solutions from the 40 000-year sequences described above, and interpolating in time between the 2 surrounding GCM solutions at any time in the long-term run. As before, the sequence of 5 GCM solutions is used in alternating directions (1 to 5, then back from 5 to 1, etc.), yielding smoothly varying eccentricity cycles with 80 000-year periodicity. After the first 40 000 years, the prescribed ice sheet extents in the GCM solutions no longer match those in the ice-model integration; i.e. we are ignoring albedo and topographic feedbacks of the ice on the large-scale climate, although the simple lapse rate corrections still capture the important height–mass balance interaction.

The importance of the opening of the Southern Ocean gateways and the formation of the ACC on EAIS mass-balance was tested by increasing the southward oceanic heat transport coefficient in the GCM by 25% over all southern latitudes, which has the effect of increasing Southern Hemispheric ocean transport by ~20%, which falls roughly in the middle of the range of responses to southern gateway changes found in prior OGCM simulations (Mikolajewicz et al., 1993; Bice et al., 2000; Nong et al., 2000; Toggweiler and Bjornsson, 2000). The resulting increase of SSTs by ~3°C around the Antarctic margin reduces net snow accumulation over the entire continent, but only slightly, with a minor effect on ice sheet mass balance, as found in prior stand-alone GCM experiments (Oglesby, 1989). With this modification to the GCM, the fully coupled 40-ky suites of runs were repeated, both for $2\times$ and $3\times CO_2$. Then, 400-ka integrations were per-

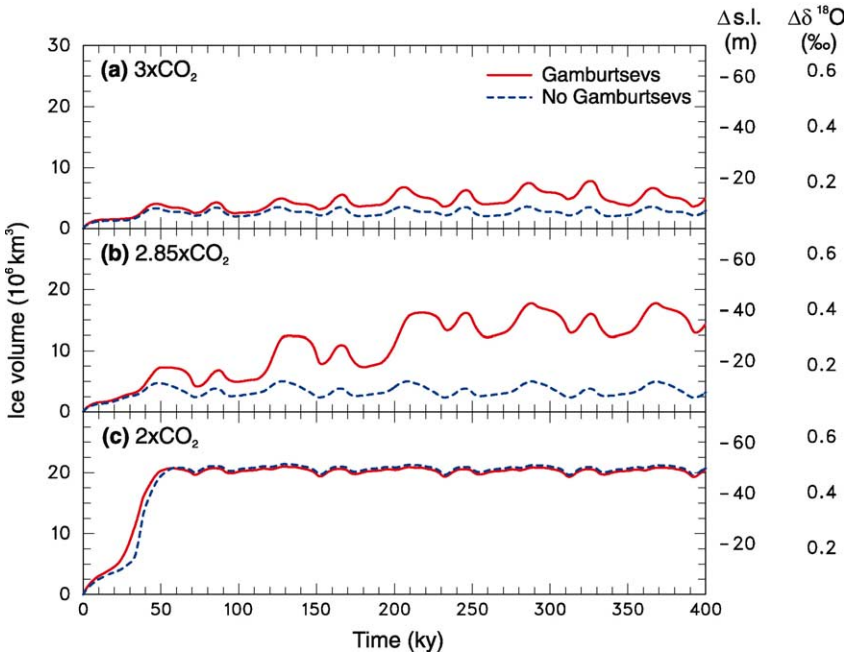

Fig. 6. As Fig. 5, except for red curves using the nominal Antarctic topography including the Gamburtsev range, and blue curves using topography modified by truncating all elevations in the Gambursev region to 1200 m above sea level.

formed as described above, for 2× and 3×CO_2, and with and without the Drake Passage modification. In addition, runs were performed representing 2.85×CO_2, using appropriately weighted means of the 2× and 3×CO_2 GCM climates at each ice sheet budget update (with the weighting allowing for the logarithmic dependence of radiative forcing on CO_2). This intermediate value is close to the critical trigger value, and shows the largest sensitivity to external perturbations. As shown in Fig. 5, the parameterized closing or opening of the Drake Passage has very little effect on ice sheet size at 2× or 3×CO_2, and only has a significant effect closer to the critical threshold value (~2.85×). Thus, the effect of an open vs. closed Drake Passage on ice sheet growth is much smaller than that caused by a drop in CO_2 from 3× to 2×, suggesting that the opening of Tasmanian and Drake Passages played a secondary role in the sudden onset of glacial conditions at 34 Ma. If the gateways opened before an EAIS had become established at ~34 Ma, then at most, they advanced the date of glacial onset slightly; if they opened after 34 Ma, as is more likely (Barker and Burrell, 1977; Lawver and Gahagan, 1998; Lawver et al., 1992), they caused the ice sheet already in existence to become only slightly larger.

3.4. 400-ka runs (Gamburtsev Mountains)

Due to their high elevations and polar location, the Gamburtsev Mountain region forms one of the first significant ice caps in our decreasing CO_2 experiments (Fig. 1) and is a likely nucleation point for glacial onset. However, the uplift history of the Gamburtsev Mountains is poorly known, and it is possible they formed after glacial onset, not before. We tested the effect of later uplift on the timing of glaciation, by re-running our 400-ka ice sheet simulations with all initial (ice-free) elevations in the Gamburtsev Mountain vicinity truncated to the elevations of the general surroundings (1200 m above sea level). Because the GCM simulations were not rerun, this modification has an effect only via the lapse-rate corrections in the ice sheet surface mass balance computations. Fig. 6 shows that the topographic

truncation has little effect on ice sheet sizes for 2× and 3× CO_2 values, and is significant only for values closer to the threshold (~2.85×). In the same way as for the Drake Passage simulations described above, the dominant effect for major ice sheet onset is a change in CO_2 from ~3× to 2×; the uplift of the Gamburtsevs, like the opening of ocean gateways, can only have a significant effect within in a relatively narrow window of atmospheric CO_2, and even then, the effect on the timing of glaciation is minor, given a scenario of gradually changing pCO_2 (DeConto and Pollard, 2003). As suggested by Mikolajewicz et al. (1993), this suggests that CO_2 is the dominant boundary condition, preconditioning the sensitivity of the climate–cryosphere system to other forcing mechanisms such as changes in ocean heat transport and mountain uplift.

4. Conclusions

The model results provide a possible explanation for the sudden build-up and subsequent variations of Antarctic ice near the Eocene–Oligocene boundary, emphasizing atmospheric CO_2, orbital forcing, and ice–climate feedbacks as the primary causes. In this scenario, CO_2 levels earlier in the Paleogene would have been high enough so that Antarctic snowline only intersected small plateaus of high topography, producing small isolated ice caps. As CO_2 continued to fall past a threshold between ~3× and 2× PAL, height–mass balance feedbacks were initiated during orbital periods producing cold austral summers (high eccentricity, low obliquity, and perihelion placing the Earth at aphelion during austral summer), allowing the ice caps to grow rapidly and respond dynamically to orbital forcing. Growing ice caps coalesced and quickly advanced over most of the East Antarctic continent, subsequently separating and shrinking during less favorable orbital periods. Orbitally forced variations in ice volume during periods of heightened sensitivity would have had a significant effect on eustatic sea level (~20 m) and the mean isotopic composition of the oceans (Figs. 5b and 6b). With further decline of CO_2 later in the Oligocene, a single, large EAIS became a more stable feature, almost insensitive to orbital forcing (Figs. 5c and 6c), with very little summer melting, and accumulation zones reaching sea level around most of the continent. While the opening of the Drake Passage and the formation of the ACC undoubtedly cooled high southern latitudes, the simulated effect on ice sheet mass balance is much smaller than expected to have occurred in the transition from 'greenhouse' to 'icehouse' climate modes, providing additional evidence for direct coupling between pCO_2 and Cenozoic climate change. The same is true for the effect of the hypothetical uplift of the Gamburtsev Mountains, which is also dependent on preexisting atmospheric CO_2 mixing ratios.

The amplified sensitivity of Antarctic ice volume to orbital forcing at levels of atmospheric CO_2 several times higher than today has important implications for our understanding of isotopic and stratigraphic proxy ice volume records, especially during presumably 'ice-free' greenhouse climate periods. Future, long-term Antarctic ice sheet stability should also be questioned, given the projected levels of atmospheric CO_2 in coming centuries.

Acknowledgements

This research was funded by the US National Science Foundation under collaborative Grant No. ATM-9905890/9906663.

References

Abe-Ouchi, A., Blatter, H., 1993. On the initiation of ice sheets. Ann. Glaciol. 18, 203–207.

Askin, R.A., 1997. Eocene–earliest Oligocene terrestrial palynology of Seymour Island, Antarctica. In: Ricci, C.A. (Ed.), The Antarctic Region: Geological Evolution and Processes, pp. 993–996.

Bamber, J.A., Bindschadler, R.A., 1997. An improved elevation dataset for climate and ice-sheet modelling: Validation with satellite imagery. Ann. Glaciol., 25.

Barker, P.F., Burrell, J., 1977. The opening of Drake Passage. Mar. Geol. 25, 15–34.

Barrett, P.J., 1996. Antarctic paleoenvironment through Cenozoic times – A review. Terra Antarct. 3, 103–119.

Barrett, P.J., Elston, D.P., Harwood, D.M., McKelvey, B.C., Webb, P.-N., 1987. Mid-Cenozoic record of glaciation and sea-level change on the margin of Victoria Land basin, Antarctica. Geology 15, 634–637.

Berger, A., Loutre, M.F., 1991. Insolation values for the climate of the last 10,000,000 years. Quat. Sci. Rev. 10, 297–317.

Berner, R.A., Kothavala, Z., 2001. Geocarb III: A revised model of atmospheric CO_2 over Phanerozoic time. Am. J. Sci. 301, 182–204.

Bice, K.L., Scotese, C.R., Seidov, D., Barron, E.J., 2000. Quantifying the role of geographic change in Cenozoic ocean heat transport using uncoupled atmosphere and ocean models. Palaeogeogr. Palaeoclimatol. Palaeoecol. 161, 295–310.

Birchfield, G.E., Weertman, J., Lunde, A.T., 1982. A model study of the role of high latitude topography in the climatic response to orbital insolation anomalies. J. Atmos. Sci. 39, 71–87.

Birkenmajer, K., Zastawniak, E., 1989. Late Cretaceous–Early Neogene vegetation history of the Antarctic Peninsula sector, Gondwana breakup and Tertiary glaciations. Bull. Pol. Acad. Sci. (Earth Sci.) 37, 63–88.

Brotchie, J.F., Sylvester, R., 1969. On crustal flexure. J. Geophys. Res. 74, 5240–5252.

Crowley, T.J., Yip, K.-J., Baum, S.K., 1994. Snowline instability in a general circulation model: Application to the Carboniferous glaciation. Clim. Dyn. 10, 363–376.

DeConto, R.M., Pollard, D., 2003. Rapid Cenozoic glaciation of Antarctica triggered by declining atmospheric CO_2. Nature 421, 245–249.

Denton, G.H., Prentice, M.L., Burckle, L.H., 1991. Cenozoic history of the Antarctica Ice sheet. In: Tingey, R.J. (Ed.), The Geology of Antarctica. Oxford University Press, Oxford, pp. 365–433.

Ehrmann, W.U., Mackensen, A., 1992. Sedimentalogic evidence for the formation of an East Antarctic ice sheet in Eocene/Oligocene time. Palaeogeogr. Palaeoclimatol. Palaeoecol. 93, 85–112.

Exon, N.F., Kennett, J.P., Malone, M.J., et al., 2001. Proceedings of the Ocean Drilling Program, Initial Reports 189. World Wide Web: http://www-odp.tamu.edu/publications/189_IR/189ir.htm.

Fitzgerald, P.G., 1992. Thermochronologic constraints on the post-Paleozoic tectonic evolution of the central Transantarctic Mountains. Tectonics 13, 818–836.

Flower, B.P., 1999. Cenozoic deep-sea temperatures and polar glaciation: The oxygen isotope record. In: Barrett, P., Orombelli, G. (Eds.), Terra Antarctica Reports 3. Terra Antarctica Publication, Siena.

Francis, J.E., 1999. Evidence from fossil plants for Antarctic paleoclimates over the past 100 million years. Terra Antarct. Rep. 3, 43–52.

Hambrey, M.J., Larsen, B., Ehrmann, W.U., 1991. The glacial record from the Prydz Bay continental shelf, East Antarctica. In: Barron, J., Larsen, B. (Eds.), Ocean Drilling Program Scientific Results 119, College Station, TX, pp. 77–132.

Hay, W.W., et al., 1999. An alternative global Cretaceous paleogeography. In: Barrera, E., Johnson, C. (Eds.), The Evolution of Cretaceous/Ocean Climate Systems. Geological Society of America, Boulder, pp. 1–48.

Huybrechts, P., 1990. A 3-D model for the Antarctic ice sheet: a sensitivity study on the glacial–interglacial contrast. Climate Dynamics 5, 79–92.

Huybrechts, P., 1993. Glaciological modelling of the Late Cenozoic East Antarctic ice sheet: Stability or dynamism? Geograf. Ann. 75, 221–238.

Kennett, J.P., 1977. Cenozoic evolution of Antarctic glaciation, the circum-Antarctic oceans and their impact on global paleoceanography. J. Geophys. Res. 82, 3843–3859.

Kerr, A., Huybrechts, P., 1999. The response of the East Antarctic ice-sheet to the evolving tectonic configuration of the Transantarctic Mountains. Glob. Planet. Change 23, 213–299.

Lawver, L.A., Gahagan, L.M., 1998. Opening of Drake passage and its impact on Cenozoic Ocean circulation. In: Crowley, T.J., Burke, K.C. (Eds.), Tectonic Boundary Conditions for Climate Reconstructions. Oxford University Press, New York, pp. 212–223.

Lawver, L.A., Gahagan, L.M., Coffin, M.F., 1992. The development of paleoseaways around Antarctica. The Antarctic Paleoenvironment: A Perspective on Global Change. Antarctic Research Series, pp. 7–30.

Lear, C.H., Elderfield, H., Wilson, P.A., 2000. Cenozoic deep-sea temperatures and global ice volumes from Mg/Ca in benthic foraminiferal calcite. Science 287, 269–272.

Maqueda, M., Willmott, A.J., Mamber, J.L., Darby, M.S., 1998. An investigation of the small ice cap instability in the Southern Hemisphere with a coupled atmosphere–sea ice–ocean–terrestrial ice model. Clim. Dyn. 14, 329–352.

Mikolajewicz, U., Maier-Reimer, E., Crowley, T.J., Kim, K.-Y., 1993. Effect of Drake and Panamanian gateways on the circulation of an ocean model. Paleoceanography 8, 409–426.

Naish, T.R. et al., 2001. Orbitally induced oscillations in the East Antarctic ice sheet at the Oligocene Miocene boundary. Nature 413, 719–723.

Nong, G.T., Najjar, R.G., Seidov, D., Peterson, W., 2000. Simulation of ocean temperature change due to the opening of Drake Passage. Geophys. Res. Lett. 27, 2689–2692.

Oglesby, R.J., 1989. A GCM study of Antarctic Glaciation. Clim. Dyn. 3, 135–156.

Pearson, P.N., Palmer, M.R., 2000. Atmospheric carbon dioxide over the past 60 million years. Nature 406, 695–699.

Pollard, D., 2000. Comparisons of ice-sheet surface mass budgets from Paleoclimate Modeling Intercomparison Project (PMIP) simulations. Glob. Planet. Change 24, 79–106.

Pollard, D., Thompson, S.L., 1997. Climate and ice-sheet mass balance at the Last Glacial Maximum from the GENESIS version 2 global climate model. Quat. Sci. Rev. 16, 841–864.

Pollard, D., DeConto, R.M., 2003. Antarctic ice and sediment flux in the Oligocene simulated by a climate–ice sheet–sediment model. Palaeogeogr. Palaeoclimatol. Palaeoecol. 10.1016/S0031-0182(03)00394-8, this volume.

Prentice, M.L., Mathews, R.K., 1991. Tertiary ice sheet dynamics: The snow gun hypothesis. J. Geophys. Res. 96, 6811–6827.

Retallack, G.J., 2002. Carbon dioxide and climate over the past 300 Myr. Philos. Trans. R. Soc. Lond. 360, 659–673.

Ritz, C., Fabre, A., Letreguilly, A., 1997. Sensitivity of a Greenland ice sheet model to ice flow and ablation parameters: Consequences for the evolution through the last climate cycle. Clim. Dyn. 13, 11–24.

Thompson, S.L., Pollard, D., 1997. Greenland and Antarctic mass balances for present and doubled atmospheric CO_2 from the GENESIS Version-2 Global Climate Model. J. Clim. 10, 871–900.

Toggweiler, J.R., Bjornsson, H., 2000. Drake Passage and paleoclimate. J. Quat. Sci. 15, 319–328.

Toggweiler, J.R., Samuels, B., 1995. Effect of Drake Passage on the global thermohaline circulation. Deep-Sea Res. 42, 477–500.

Zachos, J., Pagani, M., Sloan, L., Thomas, E., 2001. Trends, rythms, and aberrations in global climate 65 Ma to present. Science 292, 686–693.

Zachos, J.C., Breza, J.R., Wise, S.W., 1992. Early Oligocene ice sheet expansion on Antarctica: Stable isotope and sedimentological evidence from Kerguelen Plateau, southern Indian Ocean. Geology 20, 569–573.

Zachos, J.C., Quinn, T.M., Salamy, K.A., 1996. High-resolution (10^4 years) deep-sea foraminiferal stable isotope records of the Eocene–Oligocene climate transition. Paleoceanography 11, 251–266.